Title
Reduced structural connectivity of the medial temporal lobe including the perforant path is associated with aging and verbal memory impairment

Authors
Granger, Steven J
Colon-Perez, Luis
Larson, Myra Saraí
et al.

Publication Date
2023

DOI
10.1016/j.neurobiolaging.2022.10.012

Neurobiology of Aging 121 (2023) 119–128

Contents lists available at ScienceDirect

Neurobiology of Aging

journal homepage: www.elsevier.com/locate/neuaging.org

Reduced structural connectivity of the medial temporal lobe including the perforant path is associated with aging and verbal memory impairment

Steven J. Granger[a,b], Luis Colon-Perez[a,b], Myra Saraí Larson[a,b], Ilana J. Bennett[c], Michael Phelan[d], David B. Keator[e], John T. Janecek[a,b], Mithra T. Sathishkumar[a,b], Anna P. Smith[a,b], Liv McMillan[a,b], Dana Greenia[f], Maria M. Corrada[f], Claudia H. Kawas[a,b,f], Michael A. Yassa[a,b,e,f,*]

[a] Center for the Neurobiology of Learning and Memory, University of California, Irvine, CA
[b] Department of Neurobiology and Behavior, University of California, Irvine, CA
[c] Department of Psychology, University of California, Riverside, CA
[d] Department of Statistics, University of California, Irvine, CA
[e] Department of Psychiatry and Human Behavior, University of California, Irvine, CA
[f] Department of Neurology, University of California, Irvine, CA

ARTICLE INFO

Article history:
Received 17 January 2022
Revised 20 October 2022
Accepted 22 October 2022
Available online 9 November 2022

Keywords:
Perforant path
Memory
Aging
Diffusion weighted MRI
High resolution

ABSTRACT

The perforant path, the white matter bundle connecting the entorhinal cortex (ERC) with the hippocampal formation deteriorates with age-related cognitive decline. Previous investigations using diffusion-weighted MRI to quantify perforant path integrity *in-vivo* have been limited due to image resolution or have quantified the perforant path using methods susceptible to partial volume effects such as the tensor model and without consideration of its 3-dimensional morphology. In this investigation, we use quantitative-anisotropy informed tractography derived from ultra-high resolution diffusion imaging (ZOOMit) to investigate structural connectivity of the perforant path and other medial temporal lobe (MTL) pathways in older adults (63 to 98 years old, n = 51). We show that graph density within the MTL declines with age and is associated with lower delayed recall performance. We also show that older age and poorer delayed recall are associated with reduced streamlines connecting the ERC and dentate gyrus of the hippocampus (the putative perforant path). This work suggest that intra-MTL connectivity may new candidate biomarkers for age-related cognitive decline.

1. Introduction

A critical issue of neuroscience consists of characterizing structural changes in the human brain as we age. Episodic memory decline and medial temporal lobe (MTL) atrophy are markedly the most prominent and earliest pathological changes associated with age-related cognitive decline including Alzheimers Disease (Gomez-Isla et al., 1996; Price et al., 2001; Braak and Braak, 1991; Jack et al., 1999).

A key circuit of interest within the medial temporal lobe originates from the entorhinal cortex, 1 of the earliest sites of accumulation of AD-related tau pathology (Desikan et al., 2010; Desikan et 2012; Eskildsen et al., 2013). Functionally, the entorhinal cortex (ERC) has shown prominent influence in episodic memory processes as an integrating node that mediates the communication between the hippocampus and the rest of the neocortex (Reagh et al., 2018). Structurally, the entorhinal cortex is known to connect to the dentate gyrus (DG) and CA3 subfields of the hippocampus via a white matter bundle that perforates through the subiculum; the perforant path (Witter, 2007). The integrity of the perforant path is critical for normal hippocampal functioning, is vulnerable to the effects of aging, and is compromised with AD as well as normal aging (Witter et al., 1989; Witter and Amaral, 1991; Witter, 2007; Hyman et al., 1986; Yassa et al., 2010).

There have been several attempts to study this connection using non-invasive diffusion MRI which consist of studies using

* Corresponding author at: University of California, Center for the Neurobiology of Learning and Memory, 213 Qureshey Research Lab, Irvine, CA 92697, USA.
E-mail address: myassa@uci.edu (M.A. Yassa).

0197-4580/$ – see front matter © 2022 Elsevier Inc. All rights reserved.
https://doi.org/10.1016/j.neurobiolaging.2022.10.012

Table 1
Participant demographics

Variable	Full sample (n = 51)	Young-old (n = 33)	Old-old (n = 18)
Age†	80.34 ± 10.76	73.23 ± 5.48	93.39 ± 2.36
Sex	32 Females, 19 Males	21 Females, 12 Males	11 Females, 7 Males
MMSE*	26.82 ± 2.75	27.88 ± 1.52	24.89 ± 3.43
Delayed Recall Performance*	9.67 ± 3.86	11.64 ± 2.73	6.056 ± 2.90
Years of Education*	15.8 ± 2.66	16.42 ± 1.98	14.67 ± 3.36
Clinical Diagnosis	5 CIND	0 CIND	5 CIND

Key: CIND, cognitive impairment no dementia.
* Indicates statistically significant t'test between Young-old and Old-old groups.
† Indicates marginally significant difference.

ex-vivo MTL tissue samples and high angular resolution diffusion imaging (HARDI) protocols that require extensive scan times (Augustinack et al., 2010; Mollink et al., 2019; Colon- Perez et al., 2015; Beaujoin et al., 2018). Our research team has also previously demonstrated that this path can be evaluated in a rudimentary way on *in-vivo* diffusion weighted imaging (DWI) scans with sufficiently high spatial resolution (Yassa et al. 2010). While we have previously found that tensor-solved signals increase along the medial-lateral axis of the alveus which might correspond to the perforant path, the 2-dimensional nature of this method isn't sufficient to rule out other white matter that project along the anterior-posterior axis of the MTL such as the fornix, cingulum bundle, and stria terminalis. In other words, previous attempts to image the perforant pathway in studies of aging have not resolved connectivity and integrity based on respective gray matter targets of known anatomical origin consistent with perforant pathway anatomy.

In this investigation, we employ the use of a novel high-resolution (0.67 × 0.67 × 3mm) DWI (ZOOMit) sequence to quantify the structural connectivity of the MTL in a sample of 51 older adults (63 to 98 years old, 32 female). Here we utilized data from 2 separate cohorts of older adults to make up our sample, the Young-Old group (n = 33, ages 65–86, 21 Female) and the Old-Old group (n = 18, ages 90 to 98, 11 Female). To attempt to delineate the 3-dimensional structure of MTL pathways, we implemented quantitative-anisotropy informed tractography which has been shown to reduce the number of false-positive streamlines compared to a simulated ground truth in global competition (Maier-Hein, et al., 2017) and improve FA-aided deterministic tractography of phantom objects (Yeh at al., 2013). As a measure of memory performance, we focused on the Rey Auditory Verbal Learning Test (RAVLT) delayed recall performance.

We hypothesized that MTL structural connectivity would decline in older adults and in association with reduced delayed recall performance, and further, we hypothesized that perforant pathway-like connectivity (between the entorhinal cortex and dentate gyrus) would be selectively impaired in older adults and in association with reduced verbal memory performance.

2. Methods

2.1. Participants

Participants were recruited in 2 separate cohorts (Young-Old and Old-Old) at the University of California, Irvine and given appropriate compensation for their participation. Relevant demographic and RAVLT performance data are summarized in Table 1. Recruitment criteria for the Young-Old (age range 63–86) included being between the ages of 60 and 86, speak fluent English, had adequate visual and auditory acuity for neuropsychological and computerized testing, good health with no disease(s) expected to interfere with the study, willing and able to participate for the duration of the study and in all study procedures including MRI, and had normal cognition defined as a Clinical Dementia Rating of 0 and Mini-Mental State Examination Score of 27 or higher. Recruitment criteria for the Old-Old was largely the same, with the exception of testing visual and auditory acuity. Instead participants were screened for visual and auditory impairment as part of an initial medical screening. The Old-Old cohort (age range 90–98) were referred by an existing longitudinal cohort (The 90+ Study; Paganini-Hill et al., 2016) as non-demented as established by their closest visit with a neurologist. We note that approximately 5 individuals were diagnosed with Cognitive Impairment with No Dementia (CIND) from the Old-Old cohort. CIND was evaluated based on protocols from the existing longitudinal cohort study (Peltz et al., 2012). Briefly, CIND diagnosis was decided during a multidisciplinary case conferring session upon death where impairment in the memory domain or 2 or more other cognitive domains were established for diagnosis.

2.2. Imaging acquisition parameters

All neuroimaging data were acquired on a 3.0 Tesla Siemens Prisma scanner at the Facility for Imaging and Brain Research (FIBRE) at the University of California, Irvine. A high-resolution 3D magnetization-prepared rapid gradient echo (MPRAGE) structural scan (0.8mm isotropic voxels) was acquired at the beginning of each session: repetition time (TR) = 2300ms, echo time (TE) = 2.38ms, FOV =192, 256, 256mm, flip angle = 8 degrees. In addition, a T2-weighted high-resolution hippocampal sequence was acquired: TR/TE = 5000/84ms, flip angle = 17 degrees, FOV = 190, 105, 198mm, voxel size = 0.42 × 0.42 × 2.4mm. The high-resolution diffusion sequence (ZOOMit) was collected as oblique coronal slices perpendicular to the long axis of the hippocampus with the following parameters: TR/TE = 3500/75ms, FOV = 180, 71, 66mm, voxel size = 0.67 × 0.67 × 3mm. The sequence consisted of 2 b = 0 s/mm^2 volumes and a total of 60 diffusion weighted volumes acquired as 30 non-collinear directions repeated twice at a b-value of 1000 s/mm2. This sequence (ZOOMit) utilizes inner volume excitation to reduce the field of view and in-plane resolution.

2.3. Medial temporal lobe subfield segmentation in native diffusion space

T1 and T2-weighted images were used to parse the medial temporal lobe using the Automated Segmentation of Hippocampal Subfields (ASHS) pipeline to automatically label the T2-weighted images. This method implements joint label fusion, corrective learning, and is a highly accurate method in automatically deriving hippocampal subfield volumes and cortical subregions in the medial temporal lobe (Yushkevich et al., 2015). Using ASHS, the volumes for the following subregions were generated bilaterally:

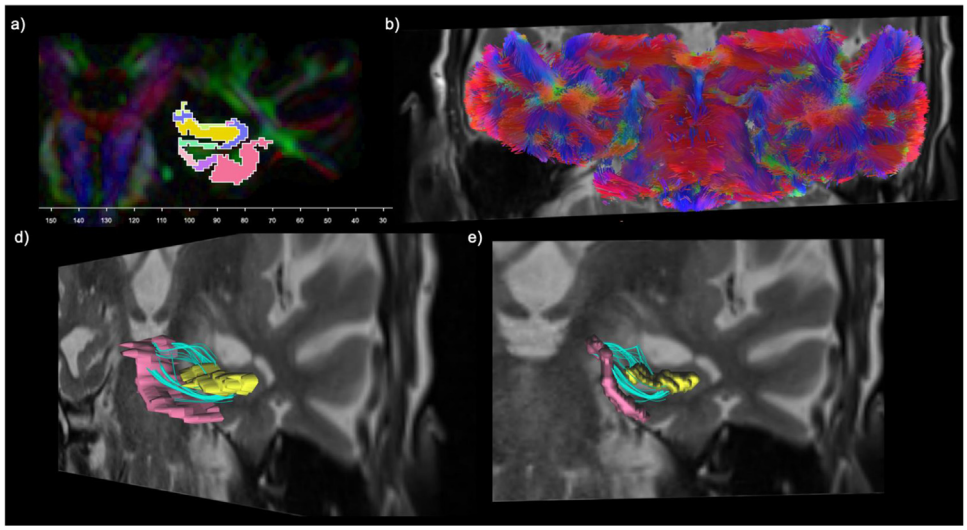

Fig. 1. QA-informed whole-brain tractography in the partial FOV high resolution GQI space. (A) Here we show a coronal section of the ASHS ROIs in the subject-specific GQI space with the entorhinal cortex (in pink) and the DG (in yellow); (B) The results of the whole brain tractography a coronal view; (C) A coronal-oblique view of the entorhinal cortex ROI (pink), and DG (yellow) for a single subject with the T2-weighted image in GQI space as the underlay. Blue streamlines here represent the streamlines that connect or 'end' in the entorhinal cortex and DG. These streamlines are representative of those extracted from the whole brain tractography generated with similar tracking parameters with the added filter of the entorhinal cortex and DG as 'end' regions through DSI-Studio's GUI interface. For interpretation of the references to color in this figure legend, the reader is referred to the Web version of this article

CA1, CA2, CA3, DG, subiculum, ERC, BA35, BA36, and PHC. The collateral sulcus and miscellaneous binary masks generated by ASHS were excluded from analysis as they represent MTL areas of non-tissue. In order to query medial temporal lobe structural connectivity, we used ANTSRegistrationSyn (Avants et al., 2009; Klein et al., 2009) to warp the T2 and associated ASHS regions to the first B0 of the partial FOV high resolution diffusion sequence (Supplementary Fig. 1). We preprocessed the ZOOMit sequence using FSLs eddy_corrrect. We quantified motion by calculating the average Euclidian distance in the linear transformation from each sub-brick to the first 2 b = 0 s/mm^2 volume prior to any motion correction.

2.4. Tractography and calculation of network measures

Tractography and network-based analyses were conducted using DSI-Studio (http://dsi-studio.labsolver.org; Fang-cheng Yeh. [2019, March 14]). The b-table was checked by an automatic quality control routine to ensure its accuracy (Schilling et al., 2019). The diffusion data were reconstructed using generalized q-sampling imaging (Yeh et al., 2010) with a diffusion sampling length ratio of 1.3. A quantitative anisotropy-informed deterministic fiber tracking algorithm (Yeh et al., 2013) was used. A seeding region was placed at the whole brain (within the partial field of view). The qa threshold was randomly selected. The angular threshold was 65 degrees. The step size was randomly selected from 0.5 voxel to 1.5 voxels. The fiber trajectories were smoothed by averaging the propagation direction with 60% of the previous direction. Tracks with length shorter than 0 or longer than 600 mm were discarded. A total of 10,000,000 seeds were placed. Topology-informed pruning (Yeh et al. 2019) was applied to the tractography with 1 iteration(s) to remove false connections. The resulting restricted FOV tractography can be visualized in Fig. 1. Observationally, the tractography generated via GQI in DSI-Studio software resulted in visually discernable structures including decussating optic chiasm. We further tested if GQI was sufficient at modeling crossing fibers by temporarily "deleting" the fibers decussating at the optic chiasm in subjects whose optic chiasm was discernable and within the field of view using DSI-Studio functions. Upon temporary deletion of the left hemisphere optic nerve, both nerves could be visualized on the other side of the optic chiasm. Upon temporary deletion of the right hemisphere optic nerve, both nerves could be visualized on the other side of the optic chiasm. This visualization technique allowed us to conclude that our diffusion sampling length ratio was appropriate in order to model crossing fibers given the normal protocol for choosing this value relies on the observation of crossing fibers at the intersection of the corticospinal tract and corpus callosum which was not available in the current field of view.

In order to query structural connectivity features of the resulting tractography we implemented DSI-Studio's use of the Brain Connectivity Toolbox (Rubinov & Spourns, 2010; https://sites.google.com/site/bctnet/). The number of streamlines 'ending' within each ASHS node pair was used as the edge weight. The average left, right, and bilateral connectivity matrices are displayed in Fig. 2. We chose to quantify graph density as a simple summary measure of overall connectedness which is calculated as the proportion of node-to-node connectivity weights that surpass an arbitrary threshold. Graph density was calculated from all ASHS nodes including the CA1, CA2, CA3, DG, subiculum, ERC, sulcus, BA35, BA36, and PHC. Four different thresholds (0.01, 0.001,0.0001,0.00001) were chosen to determine if overall "connectedness" of the MTL was associated with aging and episodic memory decline. To better understand ERC projections to the hippocampus to determine which node pair were implicated in aging and memory decline we chose the following regions: ERC, CA1, CA2, CA3, DG, and subiculum.

2.5. Neuropsychological testing

Our primary outcome measure in this investigation was performance on the Rey Auditory Verbal Learning Memory Test (RAVLT; Rey, 1964). The RAVLT is used to evaluate the quality of verbal memory and is a well-established benchmark for testing and dissociating normal aging, MCI, and Alzheimer's Disease (Estevez-Gonzalez et al., 2003). The RAVLT was administered by an examiner who was instructed to read a list of 15 words, after which the subject was asked to repeat as many words as they could remem-

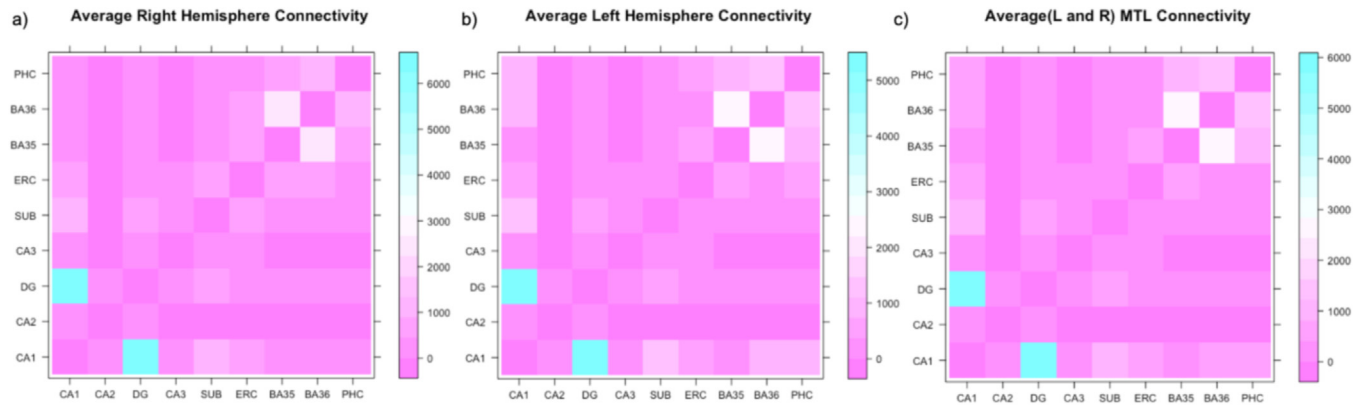

Fig. 2. Number of streamlines connecting regions within the medial temporal lobe. (A) Shows the average number of streamlines connecting right hemisphere MTL regions; (B) Shows the average number of streamlines connecting left hemisphere MTL regions;(C) Shows the averaged (left and right) hemisphere MTL connectivity. Left and right hemisphere connectivity values were averaged within individuals and then across individuals to obtain the average connectivity. All adjacency matrices are symmetric across the bottom left to top right diagonal. Visually observable is the apparently large number of streamlines connecting the CA1 and DG of the hippocampus. Other large connectivity's are between BA35 and BA36.

ber (in any order). This study/test trial was repeated for a total of 5 learning trials (Learning Trials, A1-A5) and were then followed by an immediate recall of a distractor list (B1), then immediate recall of the original list of 15 words (Immediate Recall, A6). The subject was then tested 20 minutes later making up the Delayed Recall portion. In this investigation we chose the delayed recall measure due to prior work using the tensor signal (Yassa et al., 2010) and relation to hippocampal deficits, aging and Alzheimer's Disease (Stark, 2007). In addition to Delayed Recall, we also quantified performance on the Mini-Mental State Exam (MMSE) to assess general cognitive status and include as a covariate in later regression analyses.

2.6. Statistical analysis

Statistical analyses were computed using a mixture of GraphPad Prism 7 and R Software (https://www.R-project.org/). Multiple linear regression analyses were completed using R. All correlational analyses were done using 2-tailed tests of Pearson correlation coefficients (alpha set to 0.05). ANOVA were completed using GraphPad Prism 7 and corresponding post-hoc analyses were conducted using Sidak's multiple comparisons test. Benjamini-Hochberg procedure was used to correct for multiple comparisons for node-by-node analyses (Benjamini & Hochberg, 1995).

3. Results

3.1. MTL graph density associated with age and delayed recall performance

We first sought to determine if MTL graph density within each hemisphere was dependent on the assigned arbitrary threshold. We computed graph density using 4 different thresholds (0.01, 0.001, 0.0001, 0.00001) and evaluated if the threshold impacted the connectedness of each graph. Using 2-way analysis of variance, we found a main effect of threshold ($F_{(3, 400)} = 344.2$, $p < 0.0001$; Supplementary Fig. 2). Post-hoc comparisons revealed no significant difference between left and right hemisphere graph density within each threshold. Observationally, we note that the graph density in each hemisphere reached an asymptote at 0.0001 which may possibly be too liberal of a threshold. As a result of this and the lack of difference between hemispheres, we removed analyses with graph density calculated at the smallest threshold (0.00001) and averaged graph densities across the left and right hemisphere for future analyses.

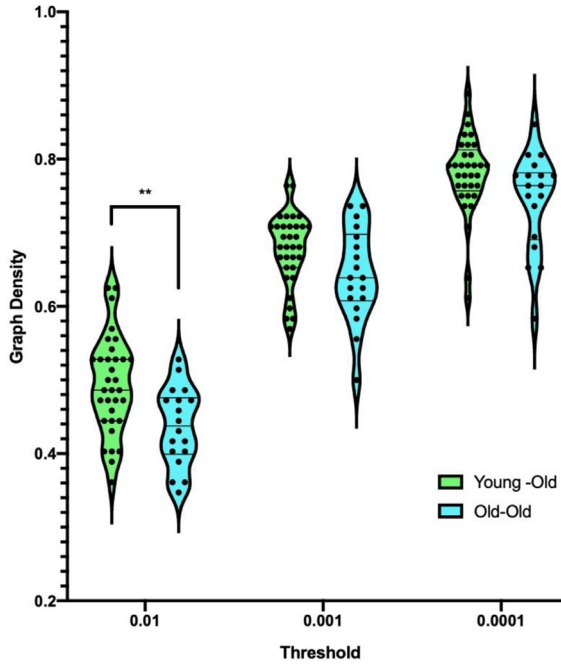

Fig. 3. Difference between Young Old and Old Old MTL Graph Density. We report a main effect of age group ($F_{(1, 147)} = 18.30$, $p < 0.0001$) and threshold ($F_{(2, 147)} = 308.8$, $p < 0.0001$). Post-hoc analysis revealed that the Old-Old cohort exhibited decreased graph density ($t = 3.32$, $p = 0.0034$) compared to the Young-Old cohort only for the 0.01 threshold.

We then tested if average MTL graph density was reduced in the Old-Old cohort compared to the Young-Old cohort. We found a main effect of age group ($F_{(1, 147)} = 18.30$, $p < 0.0001$) and a main effect of threshold ($F_{(2, 147)} = 308.8$, $p < 0.0001$). Post-hoc analyses revealed that the Old-Old cohort exhibited decreased graph density ($t = 3.32$, $p = 0.0034$) compared to the Young-Old cohort only for the 0.01 threshold (Fig. 3).

We then asked if the graph density of the MTL was associated with performance on the Delayed Recall portion of the RAVLT. We found a significant positive relation between the average graph

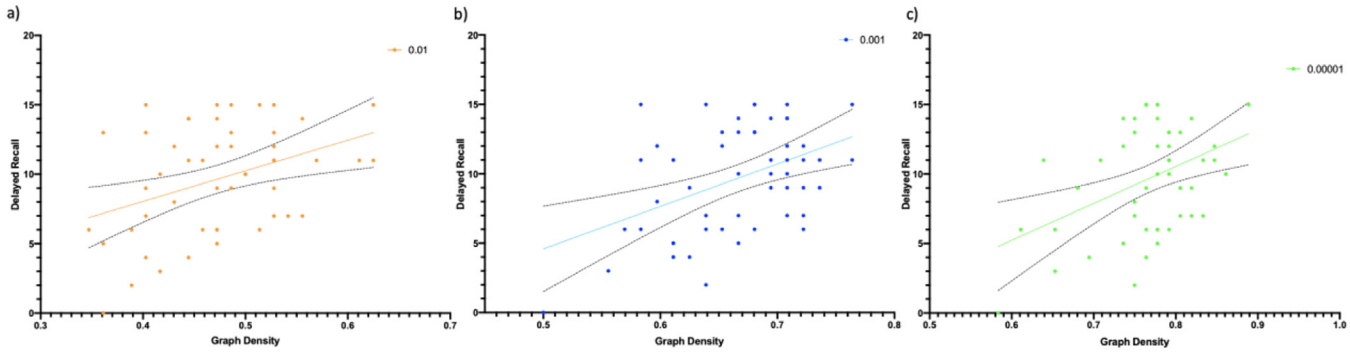

Fig. 4. Relation between MTL structural graph density and delayed recall performance. We found that the association between graph density and delayed recall was statistically significant for the (A) 0.01 threshold (r = 0.38, p = 0.0054); the (B) 0.001 threshold (r = 0.45, p = 0.001); and the (C) 0.0001 threshold (r = 0.42, p = 0.0021).

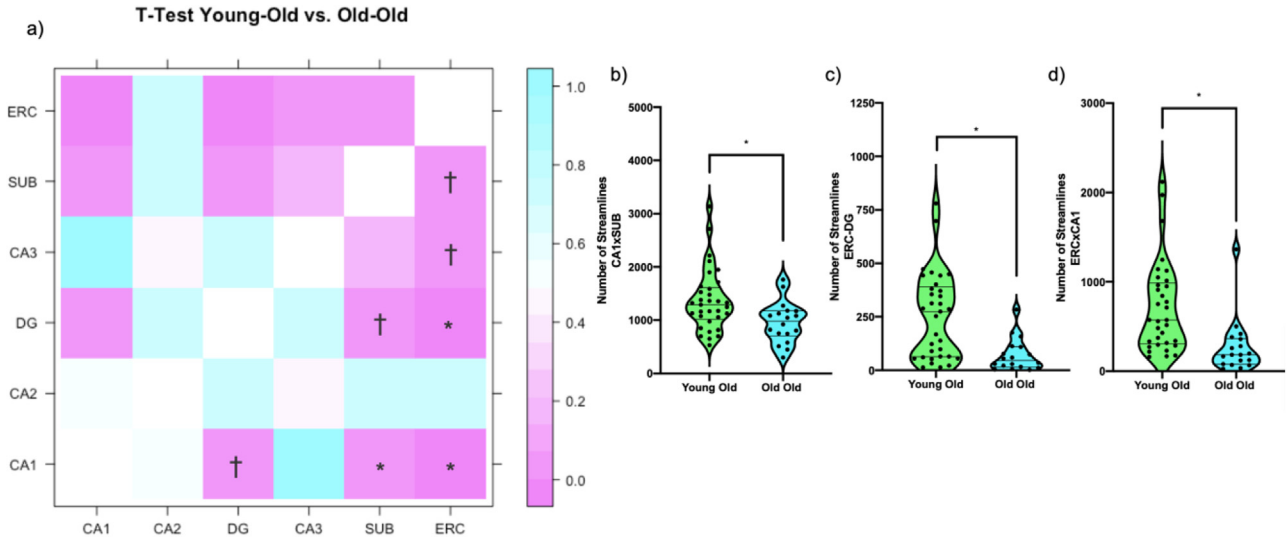

Fig. 5. Results of t'test (p-values in color) on a node-by-node basis between Young-old (n = 33) and old-old (n=18). (A) Shows all comparisons between young-old and old-old age groups; (B) shows the statistically significant difference between the CA1 and SUB connection between young-old and old-old; (C) Shows the statistically significant difference between the ERC and DG connection between young-old and old-old; (D) Shows the statistically significant difference between the connectivity of the ERC and CA1 region between young-old and old-old. *Indicate significant differences at the Benjamini-Hochberg corrected level. † indicates significant difference at the uncorrected level.

density and RAVLT Delayed Recall performance for each threshold (0.01: r = 0.38, p = 0.0054; 0.001: r = 0.45, p = 0.001; 0.0001: r = 0.42, p = 0.0021; Fig. 4).

3.2. Entorhinal cortex and dg streamlines associated with age

As a result of the differences in MTL graph density across age groups and in association with delayed recall performance, we then sought to test if there were specific connections within the MTL that were responsible for these differences. We focused on streamlines connecting the ERC with hippocampal subfields including CA1, CA2, DG, CA3, and subiculum (SUB).

We tested if there were differences between the Young-Old and Old-Old age groups on a node-by-node basis correcting for multiple comparisons using the Benjamini-Hochberg method (n = 15). Benjamini-Hochberg corrected t'tests (n = 15; Fig. 5a) revealed that the number of streamlines between the CA1-Subiculum (t = 2.69, *corrected* p = 0.048; Fig. 5b), entorhinal cortex-DG (t = 3.73, *corrected* p = 0.0074; Fig. 6c), and entorhinal cortex-CA1 (t = 3.40, *corrected* p = 0.010; Fig. 5d) were decreased in the Old-Old age group compared to the Young-Old age group.

We note here that there are several different node-by-node differences at the uncorrected level between the DG - CA1 (t = 2.14, *uncorrected* p = 0.038; Supplementary Fig. 3a), subiculum - DG (t = 2.01, *uncorrected* p = 0.047; Supplementary Fig. 3b), ERC - CA3 (t = 2.32, *uncorrected* p = 0.025; Supplementary Fig. 3c), and ERC-subiculum (t = 2.14, *uncorrected* p = 0.038; Supplementary Fig. 3d).

In addition to testing if there was a node-by-node difference across age groups, we also tested if age as a continuous variable was associated with changes in connectivity of ERC-hippocampal subfields on a node-by-node basis. After correcting for multiple comparisons, we found that age was associated with decreased structural connectivity of the entorhinal cortex – CA1 connection (r = -0.44, *corrected* p = 0.008, Supplementary Fig. 4b) as well as the entorhinal cortex – DG connection (r = -0.50, *corrected* p = 0.003; Supplementary Fig 4c).

It is possible that these differences may be biased based on a relative increase in streamlines. To address this we normalized the streamline count for each subject based on the maximum streamline (edge weight) count. The association between age (continuous) and entorhinal cortex – CA1 connectivity persisted after adjusting for the maximum graph edge weight (r = -0.36, p = 0.0086; Supplementary Fig. 5a). Similarly, the association between age and entorhinal cortex – DG connectivity persisted after adjusting for the maximum graph edge weight (r = -0.45, p = 0.0009; Supplementary Fig. 5b).

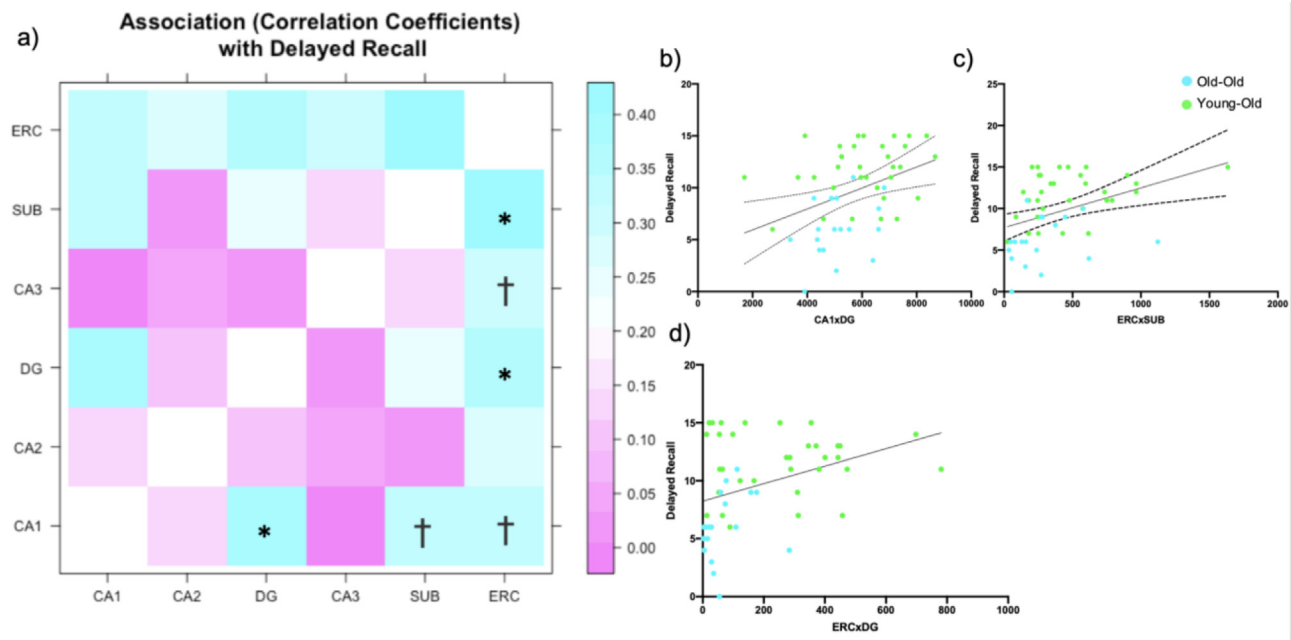

Fig. 6. Relation (correlation coefficients) between the average MTL Connectivity and delayed recall performance. (A) Shows on a node-by-node basis the correlation coefficients of the relation between node-node connectivity and RAVLT Delayed Recall Performance; (B) Shows the significant association between reduced CA1-DG structural connectivity and impaired delayed recall performance ($r = 0.38$, *uncorrected* $p < 0.01$); (C) Shows the significant association between reduced entorhinal cortex-subiculum structural connectivity and impaired delayed recall performance ($r = 0.40$, *uncorrected* $p < 0.005$); (D) Shows the significant relation between reduced entorhinal cortex-dentate gyrus structural associated with impaired delayed recall performance ($r = 0.37$, *uncorrected* $p < 0.01$). * Indicates statistically significant correlation at the Benjamini-Hochberg corrected level. † Indicates significant at the uncorrected level.

3.3. Entorhinal cortex and dg streamlines associated with delayed recall performance

We then asked if particular nodes were associated with delayed recall performance. After correcting for multiple comparisons, we found that fewer streamlines connecting the CA1 and DG ($r = 0.38$, *corrected* $p = 0.039$; Fig. 6b), entorhinal cortex and subiculum ($r = 0.40$, *corrected* $p = 0.039$; Fig. 6c), entorhinal cortex and DG ($r = 0.37$, *corrected* $p = 0.039$; Fig. 6d) were associated with reduced delayed recall performance.

The relationship between reduced CA1 and DG connectivity and reduced delayed recall performance did not persist ($\beta = 0.19$, $p = 0.11$) after accounting for MMSE, sex, years of education, and average subject in-scanner head motion (Table 2). However, the relationship between reduced entorhinal cortex – DG connectivity and reduced delayed recall performance did persist ($\beta = 0.25$, $p = 0.024$) after accounting for MMSE, sex, years of education, and subject motion (Table 3). Similarly, the relationship between reduced entorhinal cortex-subiculum structural connectivity persisted ($\beta = 0.27$, $p = 0.013$) after accounting for MMSE, sex, years of education, and subject motion (Table 4). Relationships between delayed recall and node-by-node connectivity that are statistically significant at the uncorrected level are summarized in Supplementary Fig. 6.

Similar to the node-by-node analysis with age, we then asked if the association between node pairs and delayed recall performance was driven by the graph maximum. To address this, we normalized the streamline count for each subject based on the maximum streamline (edge weight) count. We found that the relationship between entorhinal cortex – DG (r = 0.34, $p = 0.015$; Supplementary Fig. 7a) and entorhinal cortex – subiculum (r = 0.31, $p = 0.028$, Supplementary Fig. 7b) and delayed recall performance persisted after normalizing for the maximum graph edge weight. To address the possibility that a single outlying point is responsible for the positive relationship between entorhinal cortex – subiculum and delayed recall performance we removed that subject and found that the relationship between entorhinal cortex – subiculum connectivity became marginally significant (r = 0.24, $p = 0.092$). As the CA1 – DG connection was not significant after accounting for covariates and was the maximum graph edge weight for all but 5 subjects, we excluded this connection from this analysis.

3.4. Entorhinal cortex – dg connectivity moderates the association between age and delayed recall performance

As a result of the relationship between the entorhinal cortex – DG connection with age and delayed recall performance, we then asked if the entorhinal cortex – DG connectivity moderated

Table 2
Relation between CA1xDG structural connectivity and delayed recall performance does not persist after including Sex, MMSE, years of education, and average subject motion (Euclidean distance)

Regression model	R2	F	β	Standardized β	SE(β)	*p*-value
Overall Model	0.51	9.28				
Sex			-1.12	-0.14	0.88	0.21
MMSE			0.8.78	0.63	0.17	6.16×10^{-6}
Years of Education			-0.037	-0.025	0.17	0.83
CA1 x DG Connectivity			5.1×10^{-4}	0.19	3.1×10^{-4}	0.11
Euclidean Distance (prior to motion correction)			3.59	0.13	2.95	0.23

Table 3
Relation between ERCxDG structural connectivity and delayed recall performance persists after accounting for Sex, MMSE, years of education and average subject motion (Euclidean distance)

Regression model	R2	F	β	Standardized β	SE(β)	p-value
Overall Model	0.53	2.77				
Sex			-0.96	-0.12	0.84	0.26
MMSE			0.89	0.64	0.16	1.27×10^{-6}
Years of Education			-0.0054	-0.0037	0.16	0.97
ERC x DG Connectivity			0.0052	0.25	0.0022	0.024
Euclidean Distance (prior to any motion correction)			4.23	0.16	2.89	0.15

Table 4
Relation between ERCxSUB structural connectivity and delayed recall performance persists after accounting for Sex, MMSE, years of education, and average subject motion (Euclidean distance)

Regression model	R2	F	β	Standardized β	SE(β)	p-value
Overall Model	0.55	10.84				
Sex			-0.59	-0.075	0.84	0.48
MMSE			0.88	0.63	0.16	1.21×10^{-6}
Years of Education			0.038	0.026	0.16	0.82
ERC x Subiculum Connectivity			0.0032	0.27	0.0013	0.013
Euclidean Distance (prior to motion correction)			2.84	0.11	2.80	0.32

Table 5
Interaction model of Age, entorhinal cortex-dentate gyrus connectivity and their interaction predicting delayed recall performance

Regression model	R2	F	β	Standardized β	SE(β)	p-value
Overall Model	041	11.09				
Age			-0.27	-0.76	0.059	2.68×10^{-5}
ERC x DG Connectivity			-0.042	-2.064	0.020	0.044
Age ERC x DG Connectivity			0.00059	2.072	0.00027	0.034

the associated between age and delayed recall performance. We found that entorhinal cortex – DG connectivity moderated the association between age and delayed recall performance ($\beta = 2.072$, $p = 0.034$; Table 5).

4. Discussion

There are 3 major findings of this study. First, we provide evidence that structural connectivity within the MTL is reduced in the Oldest-Old and reduced MTL structural connectivity is associated with memory decline. Second, out of all possible entorhinal projections, we provide evidence that streamlines ending in the entorhinal cortex and DG are reduced in the Oldest-Old and reduced in those with memory decline. Finally, we provide evidence that entorhinal cortex - DG connectivity mediates the relationship between age and delayed recall performance.

The perforant pathway, as first visualized by Ramón y Cajal, is thought to originate in layer II and III of the entorhinal cortex and traverse the pyramidal cell layer of the subiculum in order to innervate the dentate gyrus and CA3 subfields of the hippocampal formation (Ramón y Cajal, 1911; Lorente de Nó, 1993; Witter, 2007). It is also understood that the entorhinal cortex projects to a number of other regions including the subiculum (Witter, 2006) and CA3 subfields of the hippocampus (Steward and Scoville, 1976; Witter and Amaral, 1991), as well as CA1 and CA2 regions (Desmond et al., 1994; Steward, 1976; Steward and Scoville, 1976; Witter, 2007; Naber et al., 2001; Baks-Te-Bulte et al., 2005).

Evidence from rodent studies have shown that the integrity of the perforant path declines in normal aging (Geinisman et al., 1992; Smith et al., 2000). Histological studies from *ex-vivo* human data suggest that perforant path integrity is associated with AD-pathology (Hyman et al., 1986) and is compromised in those with mild cognitive impairment (Scheff et al., 2006). Extending these findings, using histology from *ex-vivo* human data, our colleagues have shown that perforant path synaptic loss is related to cognitive impairment and AD-pathology in humans over 90 years old (Robinson et al., 2014).

With the goal of translating these findings to create an early and detectable biological marker of age-related cognitive decline, our laboratory was the first to measure perforant path integrity using *in-vivo* ultra-high-resolution diffusion weighted imaging targeted at the medial temporal lobe. In this investigation, we used a submillimeter diffusion-weighted imaging sequence to detect anisotropy along the orientation of the perforant path using a composite measure of tensor-derived signals (Yassa et al., 2010). Using this method, we were able to show that the diffusion strength of the perforant path (compared across the medial-lateral axis of the medial temporal lobe) decreased in older adults. As a control, we selected the alveus (forming the anterior portion of the fimbria/fornix), which did not show the same decrease in diffusion parameters associated with age and memory impairment. Critically, this finding improved previous work that did not utilize sufficiently high voxel resolution to observe the perforant path (Kalus et al., 2006; Rogalski et al., 2009). While our prior work was the first investigation of diffusion anisotropy of the perforant path *in-vivo* and provided an association with aging and episodic memory performance, others in the field have suggested that this method partially or indirectly captures the perforant pathway (Zeineh et al., 2012) based on its consideration of the perforant path in the 2-dimensional coronal plane rather than with respect to the 3-dimensional morphology of this pathway. In other words, our previous attempt to image the perforant pathway did not resolve connectivity and integrity based on respective gray matter targets of known anatomical origin consistent with perforant pathway anatomy.

In the last decade, other researchers in the field have begun to address these issues using tractography. The perforant path has now been investigated using excised human and non-human primate tissue scanned with high angular resolution diffusion imag-

ing (HARDI) protocols at high magnetic field strengths to resolve 3-dimensional images of the perforant path (Augustinack et al., 2010; Mollink et al., 2019; Colon- Perez et al., 2015; Beaujoin et al., 2018; Zeineh et al., 2017). A smaller number of studies have investigated the perforant path in humans using *in-vivo* tractography derived from high-resolution diffusion imaging. One such study implemented high-resolution diffusion imaging to visualize the perforant path using fractional anisotropy-aided deterministic tractography (Zeineh et al., 2012). In this investigation, using resampled 1.5mm isotropic data (final resolution 0.7mm isotropic) from 6 human subjects, the authors were able to visualize the perforant path *in-vivo* operationalized as streamlines connecting the entorhinal cortex with the DG/CA3, CA1, and subiculum.

While this investigation provided 1 of the first *in-vivo* 3-dimensional visualizations of entorhinal-hippocampal projections in the high-resolution space, the question remains as to which specific entorhinal-hippocampal projection declines with age and memory decline. To address this issue in this investigation, we focused on improving the existing tractography work, by implementing quantitative anisotropy (QA) informed deterministic tractography (Yeh et. al., 2013). It has been shown that QA-informed tractography improves the accuracy of deterministic tractography of microtubule phantom objects and is less affected by partial volume effects compared to the tensor model (Yeh et al., 2013). In addition, the use of quantitative anisotropy was found to produce fewer false-positive streamlines compared to over 96 different methods released by more than 20 other research groups around the world (Maier-Hein, 2017). In this investigation, by employing the use of generalized q-sampling (GQI) imaging, QA-aided deterministic tractography in the native diffusion space and seeding the high resolution sequence with 10,000,000 seeds (10x the suggest amount for whole brain analysis), we were able to generate a robust model of structural connectivity (Fig. 1a). This was made possible by the use of the high-resolution diffusion imaging sequence (ZOOMit; voxel size = 0.67 × 0.67 × 3mm) acquired parallel to the long axis of the hippocampus. This robust tractography derived from ZOOMit, along with acquisition of high-resolution T1 and T2-weighted imaging data, allowed for harmonization with ASHS to delineate MTL regions (see methods). Together, this harmonization approach allowed us to quantify the number of streamlines ending between MTL regions in order to determine which *specific* entorhinal projection was associated with aging and memory decline.

Using these methods to improve upon prior work, we provide evidence that MTL structural connectedness (graph density) was reduced in those at advanced age. Interestingly, this difference was only apparent for the most restrictive arbitrary threshold of 0.01. Here it is possible that the difference is only apparent at this more restrictive threshold as it might contribute to the removal of spurious streamlines of low count across the network. However, we provide evidence that reduced MTL structural connectedness (across all thresholds) was associated with reduced RAVLT delayed recall performance. Together these results seem to suggest that the degree of white matter connecting the medial temporal lobe is an additional indicator of age-related cognitive decline.

As a result of this first analysis, we then asked which specific entorhinal projections to the subiculum and hippocampal formation were more vulnerable to the effects of aging and cognitive decline. We found that the connectivity of the CA1-subiculum, entorhinal cortex- DG, and entorhinal cortex-CA1 were diminished in those at advanced age. Similarly, we then asked which specific connections between the entorhinal cortex and hippocampal formation were associated with episodic memory decline. We found that reduced connectivity between the CA1 - DG, entorhinal cortex-subiculum, and the entorhinal cortex -DG was related to impaired delayed recall performance. However, only the relationships between memory performance and entorhinal cortex-subiculum and entorhinal cortex – DG persisted after accounting for sex, MMSE, years of education, and average subject head motion. These relationships also persisted after accounting for the maximum subject streamline count. Here we note that our usage of the terminology 'persists' refers to the ability of the connectivity regressor and corresponding p-value to surpass our arbitrary threshold of alpha. A more general interpretation of these results would suggest that entorhinal – DG connectivity is associated with delayed recall performance when MMSE, years of education, and motion are accounted for. Importantly, we note that the entorhinal cortex – DG projection is the *only node-to-node connection that is both reduced in the Oldest-Old and is reduced in those with episodic memory decline*.

We have previously reviewed the functional significance of different entorhinal projections in the context of computational theories of DG and CA3 functioning (Yassa & Stark, 2011). It is hypothesized that the direct entorhinal projection to the DG provides input for sparse coding granule cells of the DG to perform pattern separation; a process whereby input is orthogonalized to create unique representations. These newly separated representations are then "collected" by CA3 to reduce interference and support new learning through the mossy fiber pathway (Marr, 1971; Blackstad et al., 1970; Yassa & Stark, 2011). The direct entorhinal projection to CA3 is thought to provide a cue for recall (Rolls, 2007). This theory has been supported by selective lesioning of the mossy fiber pathway which impaired encoding but not retrieval where lesioning of the direct entorhinal – CA3 pathway impaired retrieval but spares encoding (Lee & Kesner, 2004; Yassa & Stark, 2011). Thus, it is tempting to speculate that our findings of reduced entorhinal cortex- DG connectivity would yield impairment in encoding new representations or impairment of pattern separation processes. Indeed, additional research using the fractional anisotropy methodology we have previously developed (Yassa et al., 2010) has found that the perforant path integrity is associated with discrimination performance (Bennett & Stark, 2016; Yassa et al., 2011). However, this work is also subjected to the criticism laid out by Zeineh et al. (2012) as it does not measure the perforant pathway with respect to its gray matter targets and 3-dimensional morphology. Rather, diffusion was accessed locally between the entorhinal cortex and subiculum at a 45-degree angle. Here, we extend this body of work by providing the novel finding that entorhinal cortex – DG streamlines, in particular, decline with aging and are associated with episodic memory performance.

One limitation of this work is that we observed the largest streamline count for most subjects between the CA1 and DG which anatomically is not thought to have a reciprocal connection. In general, future studies should seek to compare the accuracy of streamlines derived from high-resolution diffusion imaging with histological methods from *ex-vivo* samples that implement anterograde and retrograde tracing. In animal models, 1 such study has been conducted recently that compared *in-vivo* 0.1mm resolution tractography with *ex-vivo* viral tracing (Wu & Zhang, 2016). This investigation found evidence of remarkable similarity between tractography and the viral tracer data in terms of their spatial projection patterns, and also found false positive streamline connectivity between the CA1 and DG of the hippocampus (Wu & Zhang, 2016). Similar techniques should be employed with excised human tissue with the high-resolution sequence to better understand the 3-dimensional accuracy of this work.

Another possible limitation of this work is the use of a single shell (single b-value) DWI sequence. It is possible that the implementation of the ZOOMit high resolution sequence adapted to include a multishell diffusion weighted imaging would enhance the tractography results. It is possible that this adaptation would en-

able the quantification of separate streamlines projecting from different portions of the entorhinal cortex such as the lateral ("content") and medial ("context") pathways which are known to support different functions (Knierim et al., 2013; Reagh & Yassa, 2014).

5. Conclusion

In this investigation we provide evidence that the number of streamlines that connect the entorhinal cortex and DG are associated with aging and episodic memory performance. These analyses advance the study of white matter within the medial temporal lobe by supplying 3-dimensional specificity to our previous work (Yassa et al., 2010). Future study should seek to determine if multishell acquisition would be able to yield direct visualization of the perforant path using similar state-of-the-art MTL segmentation and tractography procedures.

Disclosure statement

The authors have no actual or potential conflicts of interest.

Author Contributions

S.J.G., C.H.K., and M.A.Y. designed the research, S.J.G., M.S.L., M.T.S., A.P.S., L.M., D.G., and M.M.C. performed the research, L.C-P., J.T.C., M.P. and D.B.K. contributed analytic tools, S.J.G. analyzed data, S.J.G. drafted the initial version of the paper, S.J.G. and M.A.Y. wrote the paper with input from all of the authors.

Supplementary materials

Supplementary material associated with this article can be found, in the online version, at doi:10.1016/j.neurobiolaging.2022.10.012.

References

Augustinack, J.C., Helmer, K., Huber, K.E., Kakunoori, S., Zöllei, L., Fischl, B., 2010. Direct visualization of the perforant pathway in the human brain with ex vivo diffusion tensor imaging. Frontiers of Human Neuroscience 4 (42).

Avants, B.B., Tustison, N., Song, G., 2009. Advanced normalization tools (ANTS). Penn Image Computing and Science Laboratory; University of Pennsylvania, Philadelphia.

Baks-Te-Bulte, L., Wouterlood, F.G., Vinkenoog, M., Wit-ter, M.P., 2005. Entorhinal projections terminate onto principal neurons and interneurons in the subiculum: aquantitative electron microscopical analysis in the rat. Neuroscience. 136 (3), 729–739.

Beaujoin, J., Palomero-Gallagher, N., Boumezbeur, F., Axer, M., Bernard, J., Poupon, F., Schmitz, D., Mangin, J.-F., Poupon, C., 2018. Post-mortem inference of the human hippocampal connectivity and microstructure using ultra-high field diffusion MRI at 11.7 T. Brain Struct Funct 223, 2157–2179.

Benjamini, Y., Hochberg, Y., 1995. Controlling the false discovery rate: a practical and powerful approach to multiple testing. J Royal Stat Soc Series B 57, 289–300.

Bennett, I.J., Stark, C.E., 2016. Mnemonic discrimination relates to perforant path integrity: An ultra-high resolution diffusion tensor imaging study. Neurobiol Learn Mem 129, 107–112.

Blackstad, T.W., Brink, K., Hem, J., Jeune, B., 1970. Distribution of hippocampal mossy fibers in the rat. An experimental study with silver impregnation methods. J Comparat Neurol 138 (4), 433–449.

Braak, H., Braak, E., 1991. Neuropathological stageing of Alzheimer-related changes. Acta Neuropathol 82, 239–259.

Colon-Perez, L.M., King, M., Parekh, M., Boutzoukas, A., Carmona, E., Couret, M., Carney, P.R., 2015. High-field magnetic resonance imaging of the human temporal lobe. NeuroImage: clinical 9, 58–68.

Desikan, R.S., McEvoy, L.K., Thompson, W.K., Holland, D., Brewer, J.B., Aisen, P.S., et al., 2012. Amyloid-β–associated clinical decline occurs only in the presence of elevated P-tau. Arch Neurol. 69, 709–713.

Desikan, R.S., Sabuncu, M.R., Schmansky, N.J., Reuter, M., Cabral, H.J., Hess, C.P., et al., 2010. Selective disruption of the cerebral neocortex in Alzheimer's disease. PLoS One 5, e12853.

Desmond, N.L., Scott, C.A., Jane, J.A., Levy, W.B., 1994. Ultrastructural identification of entorhinal cortical synapsesin CA1 stratum lacunosum-moleculare of the rat. Hippo-Campus 4 (5), 594–600.

Eskildsen, S.F., Coupé, P., García-Lorenzo, D., Fonov, V., Pruessner, J.C., Collins, D.L., 2013. Prediction of Alzheimer's disease in subjects with mild cognitive impairment from the ADNI cohort using patterns of cortical thinning. NeuroImage 65, 511–521.

Estévez-González, A., Kulisevsky, J., Boltes, A., Otermín, P., García-Sánchez, C., 2003. Rey verbal learning test is a useful tool for differential diagnosis in the preclinical phase of Alzheimer's disease: comparison with mild cognitive impairment and normal aging. International journal of geriatric psychiatry 18 (11), 1021–1028.

Geinisman, Y., deToledo-Morrell, L., Morrell, F., Persina, I.S., Rossi, M., 1992. Age-related loss of axospinous synapses formed by two afferent systems in the rat dentate gyrus as revealed by the unbiased stereological dissector technique. Hippocampus. 2, 437–444.

Gomez-Isla, T., Price, J.L., McKeel, D.W.J., Morris, J.C., Growdon, J.H., Hyman, B.T., 1996. Profound loss of layer II entorhinal cortex neurons occurs in very mild Alzheimer's disease. Neuroscience. 16, 4491–4500.

Hyman, B.T., Van Hoesen, G.W., Kromer, L.J., Damasio, A.R., 1986. Perforant pathway changes and the memory impairment of Alzheimer's disease. Ann neurol 20 (4), 472–481.

Jack, C.R., Petersen, R.C., Xu, Y.C., O'Brien, P.C., Smith, G.E., Ivnik, R.J., Boeve, B.F., Waring, S.C., Tangalos, E.G., 1999. Kokmen E. Prediction of AD with MRI-based hippocampal volume in mild cognitive impairment. Neurology 52, 1397–1403.

Kalus, P., Slotboom, J., Gallinat, J., Mahlberg, R., Cattapan-Ludewig, K., Wiest, R., Nyffeler, T., Buri, C., Federspiel, A., Kunz, D., Schroth, G., Kiefer, C., 2006. Examining the gateway to the limbic system with diffusion tensor imaging: the perforant pathway in dementia. NeuroImage 30 (3), 713–720.

Klein, A., Andersson, J., Ardekani, B.A., Ashburner, J., Avants, B., Chiang, M.C., Christensen, G.E., Collins, D.L., Gee, J., Hellier, P., Song, J.H., Jenkinson, M., Lepage, C., Rueckert, D., Thompson, P., Vercauteren, T., Woods, R.P., Mann, J.J., Parsey, R.V., 2009. Evaluation of 14 nonlinear deformation algorithms applied to human brain MRI registration. NeuroImage 46 (3), 786–802.

Knierim, J.J., Neunuebel, J.P., Deshmukh, S.S., 2013. Functional correlates of the lateral and medial entorhinal cortex: Objects, path integration and local-global reference frames. Philos Trans R Soc Lond B Biol Sci. 369, 20130369.

Lee, I., Kesner, R.P., 2004. Encoding versus retrieval of spatial memory: double dissociation between the dentate gyrus and the perforant path inputs into CA3 in the dorsal hippocampus. Hippocampus 14 (1), 66–76.

Lorente de No R., 1933. Studies on the structure of the cer-ebral cortex. J Psychol Neurol. 45 (6), 26–438.

Maier-Hein, K.H., Neher, P.F., Houde, J.C., Côté, M.A., Garyfallidis, E., Zhong, J., Descoteaux, M., 2017. The challenge of mapping the human connectome based on diffusion tractography. Nature Communications 8 (1), 1349.

Marr, D., 1971. Simple memory: a theory for archicortex. Philos Trans R Soc Lond B Biol Sci. 262, 23–81.

Mollink, J.M.H., Miller, K.L., Huszar, I.N., Jenkinson, M., Raaphorst, J., Wiesmann, M., Ansorge, O., Pallebage-Gamarallage, M., van Cappellen van Walsum, A.M., 2019. White matter changes in the perforant path area in patients with amyotrophic lateral sclerosis. Neuropathol Appl Neurobiol 45 (6), 570–585.

Naber, P.A., Lopes da Silva, F.H., Witter, M.P., 2001. Reciprocal connections between the entorhinal cortex and hippocampal fields CA1 and the subiculum are in register with the projections from CA1 to the subiculum. Hippocampus 11 (2), 99–104.

Paganini-Hill, A., Kawas, C.H., Corrada, M.M., 2016. Lifestyle factors and dementia in the oldest-old: the 90+ study. Alzheimer Dis Assoc Disord 30 (1), 21–26.

Peltz, C.B., Corrada, M.M., Berlau, D.J., Kawas, C.H., 2012. Cognitive impairment in nondemented oldest-old: prevalence and relationship to cardiovascular risk factors. Alzheimer Dis Assoc Disord 8 (2), 87–94.

Price, J.L., Ko, A.I., Wade, M.J., Tsou, S.K., McKeel, D.W., Morris, J.C., 2001. Neuron number in the entorhinal cortex and CA1 in preclinical Alzheimer disease. Arch Neurol. 58, 1395–1402.

R Core Team. R: a language and environment for statistical computing.

Ramón y Cajal, S., 1911. Histologie du SystemeNerveux del'Homme et des Vertebres. Maloine, Paris.

Reagh, Z.M., Yassa, M.A., 2014. Object and spatial mnemonic interference differentially engage lateral and medial entorhinal cortex in humans. Proc Natl Acad Sci U S A 111 (40), E4264–E4273.

Reagh, Z.M., Noche, J.A., Tustison, N.J., Delisle, D., Murray, E.A., Yassa, M.A., 2018. Functional imbalance of anterolateral entorhinal cortex and hippocampal Dentate/CA3 underlies age-related object pattern separation deficits. Neuron 97 (5), 1187–1198.e4.

Rey A., 1964. L'examen clinique en psychologie. Presses Universitaires de France, Paris.

Robinson, J.L., Molina-Porcel, L., Corrada, M.M., Raible, K., Lee, E.B., Lee, V.M.Y., Trojanowski, J.Q., 2014. Perforant path synaptic loss correlates with cognitive impairment and Alzheimer's disease in the oldest-old. Brain 137 (9), 2578–2587.

Rogalski, E.J., Murphy, C.M., deToledo-Morrell, L., Shah, R.C., Moseley, M.E., Bammer, R., Stebbins, G.T., 2009. Changes in parahippocampal white matter integrity in amnestic mild cognitive impairment: a diffusion tensor imaging study. Behav Neurol 21 (1), 51–61.

Rolls, E.T., 2007. An attractor network in the hippocampus: theory and and neurophysiology. Learn Mem. 14, 714–731.

Rubinov, M., Sporns, O., 2010. Complex network measures of brain connectivity: uses and interpretations. NeuroImage. 52, 1059–1069.
Scheff, S.W., Price, D.A., Schmitt, F.A., Mufson, E.J., 2006. Hippocampal synaptic loss in early Alzheimer's disease and mild cognitive impairment. Neurobiol Aging 27 (10), 1372–1384.
Schilling, K.G., et al., 2019. A fiber coherence index for quality control of B-table orientation in diffusion MRI scans. Magn Reson Imaging 58, 82–89.
Smith, T.D., Adams, M.M., Gallagher, M., Morrison, J.H., Rapp, P.R., 2000. Circuit-specific alterations in hippocampal synaptophysin immunoreactivity predict spatial learning impairment in aged rats. J Neurosci. 20, 6587–6593.
Stark, C.E.L., 2007. Functional role of the human hippocampus. In: Andersen, P., Morris, R., Amaral, D., Bliss, T., O'Keefe, J. (Eds.), The Hippocampus Book. Oxford University Press, New York, pp. 549–579.
Steward, O., 1976. Topographic organization of the projectionsfrom the entorhinal area to the hippocampal formation of therat. J Comp Neurol. 167 (3), 285–314.
Steward, O., Scoville, S.A., 1976. Cells of origin of ent-orhinal cortical afferents to the hippocampus and fascia den-tata of the rat. J Comp Neurol 169 (3), 347–370.
Witter, M.P., 2007. The perforant path: projections from the entorhinal cortex to the dentate gyrus. Prog Brain Res 163, 43–61.
Witter, M.P., 2006. Connections of the subiculum of the rat: topography in relation to columnar and laminar organization. Behav Brain Res. 174 (2), 251–264.
Witter, M.P., Groenewegen, H.J., Lopes da Silva, F.H., Lohman, A.H., 1989. Functional organization of the extrinsic and intrinsic circuitry of the parahippocampal region. Prog Neurobiol. 33 (3), 161–253.
Witter, M.P., Amaral, D.G., 1991. Entorhinal cortex of the monkey. V. Projections to the dentate gyrus, hippocampus, and subicular complex. J Comp Neurol 307 (3), 437–459.
Wu, D., Zhang, J., 2016. In vivo mapping of macroscopic neuronal projections in the mouse hippocampus using high-resolution diffusion MRI. NeuroImage 125, 84–93.
Yassa, M.A., Mattfeld, A.T., Stark, S.M., Stark, C.E.L., 2011. Age-related memory deficits linked to circuit-specific disruptions in the hippocampus. Proc Nat Acad Sci 108 (21), 8873–8878.
Yassa, M.A., Muftuler, L.T., Stark, C.E.L., 2010. Ultrahigh-resolution microstructural diffusion tensor imaging reveals perforant path degradation in aged humans in vivo. Proc Nat Acad Sci 107 (28), 12687–12691.
Yeh, F.-C., 2019. DSI Studio (Version 2019 March). Zenodo.
Yeh, F.C., Panesar, S., Barrios, J., Fernandes, D., Abhinav, K., Meola, A., Fernandez-Miranda, J.C., 2019. Automatic removal of false connections in diffusion mri tractography using topology-informed pruning (TIP). Neurotherapeutics 1, 52–58.
Yeh, F.C., Verstynen, T.D., Wang, Y., Fernández-Miranda, J.C., Tseng, W.Y.I., 2013. Deterministic diffusion fiber tracking improved by quantitative anisotropy. PLoS ONE 8 (11), 1–16.
Yeh, F.-C., Wedeen, V.J., Tseng, W.-Y.I., 2010. Generalized-sampling imaging."Medical Imaging. IEEE Trans Med Imaging. 29 (9), 1626–1635.
Yushkevich, P.A., Pluta, J.B., Wang, H., Xie, L., Ding, S., Gertje, E.C., Mancuso, L., Kliot, D., Das, S.R., Wolk, D.A., 2015. Automated volumetry and regional thickness analysis of hippocampal subfields and medial temporal cortical structures in mild cognitive impairment. Hum Brain Mapp 36, 258–287.
Zeineh, M.M., Holdsworth, S., Skare, S., Atlas, S.W., Bammer, R., 2012. Ultra-high resolution diffusion tensor imaging of the microscopic pathways of the medial temporal lobe. NeuroImage 62 (3), 2065–2082.
Zeineh, M.M., Palomero-Gallagher, N., Axer, M., Gräßel, D., Goubran, M., Wree, A., Woods, R., Amunts, K., Zilles, K., 2017. Direct visualization and mapping of the spatial course of fiber tracts at microscopic resolution in the human hippocampus. Cereb Cortex 27 (3), 1779–1794.